ELSEVIER

Thin Solid Films 414 (2002) 1–6

thin solid films

www.elsevier.com/locate/tsf

Characterization of porous silicate for ultra-low *k* dielectric application

Po-tsun Liu[a,*], T.C. Chang[a,b], K.C. Hsu[c], T.Y. Tseng[c], L.M. Chen[d], C.J. Wang[d], S.M. Sze[a,c]

[a]*National Nano Device Laboratory, 1001-1 Ta-Hsueh Road, HsinChu 300, Taiwan*
[b]*Department of Physics, National Sun Yat-Sen University, Kaohsiung 80424, Taiwan*
[c]*Institute of Electronics, National Chiao Tung University, HsinChu 300, Taiwan*
[d]*Union Chemical Laboratories, Industrial Technology Research Institute, HsinChu 300, Taiwan*

Received 23 April 2001; received in revised form 11 April 2002; accepted 12 April 2002

Abstract

Thermal stability of a porous low-*k* film is a critical issue for application consideration in the back-end-of-line. In this study, thermal stability of the porous silicate has been investigated by changing the thermal processing temperatures. Experimental results have shown that the dielectric constant of the porous silicate still remains below 2.0 after thermal processing at 500 °C for 1 h. A series of material analysis techniques and electrical characteristics have been used to verify the physical and chemical characteristics of the porous silicate film. © 2002 Elsevier Science B.V. All rights reserved.

Keywords: Dielectric constant; Porous silicate films; Thermal stability

1. Introduction

As devices scale down to a deep sub-micron regime for fast switching speeds, the interconnect resistance–capacitance delay becomes increasingly dominant over intrinsic gate delay [1,2]. Power dissipation and noise crosstalk also have received considerable attention in the deep sub-micron regime due to the decrease in wiring dimensions and pitches. Using metal lines with low resistivity and on-chip insulators with low dielectric constant (low-*k*) as an interconnect architecture will mitigate these issues [3].

Recently, the conventional aluminum wiring has been replaced by copper, resulting in a 40% decrease in the metal interconnect resistivity. However, progress in low-*k* dielectrics is complicated. Many low-*k* candidates are developed by either chemical vapor deposition techniques or spin-on procedures, as shown in Refs. [4–7]. It is found that there is a plethora of candidates with dielectric constant in the 2.5–3.0 range. These include both inorganic or organic silicates as well as organic polymers. As features sizes in integrated circuits (IC) approach 0.1 μm, however, it is necessary to reduce the dielectric constant of the dielectrics below 2.0 [3]. This means these dielectric materials will need to be produced in a porous form.

The silicate-based porous materials including xerogels and aerogels are highly promising candidates for advanced interconnects. Their adjustable dielectric properties make porous silicate suitable for different IC technology nodes [8–10]. As a good intermetal dielectric for use in the back-end-of-line, the porous silicate must have several properties including a low dielectric constant, good thermal stability, electrical characteristics, and low moisture uptake [11].

In this study the chemical, electrical characteristics and thermal stability of porous silicate which was manufactured by Industrial Technology Research Institute Chemical Laboratory have been investigated comprehensively.

2. Experimental

The precursor solution of porous silicate used in this work was prepared by mixing tetraethoxylane (TEOS) with a base catalyst and organic additives at room temperature. The composition of the sol was TEOS/H_2O/NH_4OH/CH_3OH in a 1:2.5:0.5:50 molar ratio. Following the sol preparation, sol was spun on 4-in. p-

*Corresponding author. Tel.: +886 3 572610; fax: +886 3 5722715.
E-mail address: ptliu@ndls.gov.tw (P.-t. Liu).

PII: S0040-6090(02)00423-6

type wafers (resistivity: 15–20 Ω cm) with (1 0 0) orientation. The spin process was divided into 4 steps. The first step (200 rpm/5 s), which was fully established before dripping the sol solution, was beneficial for sequent sol spreading. In the second step (500 rpm/6 s), 10 ml of sol was dripped on wafers. The third step (1500 rpm/10 s) was a rinsing stage designed to get rid of the edge bead of precursor, which might induce crack when drying. Finally, the fourth step (1000 rpm/20 s) removed the residual solvent by spinning dying. After spin deposition, the sol–gel film was immersed in trimethylchlorosilane (TMCS; $(CH_3)_3SiCl$) atmosphere at 60 °C for 30 min. Surface modification with TMCS was beneficial to sol–gel drying since TMCS can react with Si–OH bonds on the surface of SiO_2 gel and replace them with –Si–O–Si(CH_3) bonds [12]. The hydroxylated surface of SiO_2 gel was thereby changed with organosilanes ($-Si(CH_3)_3$) after the surface modification. The wafers were finally placed on hot plates for a sequence of pre-baking at 80 °C for 1 min and 150 °C for 1 min. The wafers were then cured at 400 °C in a furnace under nitrogen atmosphere for 1 h. The investigation on the thermal stability of the porous silicate was carried out by annealing under nitrogen atmosphere at temperatures ranging from 350 to 600 °C for 1 h.

The refractive index and thickness of the porous silicate were measured with a commercially available instrument named as n&k analyzer, supplied by a company called n&k Technology. The porosity and average pore size of the porous silicate were studied through N_2 adsorption/desorption isotherm analysis. The porosity of the as-cured porous film is approximately 70% (volume percentage) with an average pore size of 2 nm. The chemical structure of the porous silicate was determined by Fourier transform infrared spectrometry (FTIR Bio-Red QS300), which was performed from 400 to 4000 cm^{-1}. Electrical measurements were conducted on metal insulator semiconductor (MIS) capacitors. Al electrodes were evaporated on the front surface of the films and the backside of the substrate. The capacitance was measured at 1 MHz with an AC bias using a Keithley Model 82 CV meter. The current–voltage (I–V) characteristics were measured with an HP4145B semiconductor parameter analyzer with the MIS capacitor biased at the accumulation polarity. Material analysis using thermal desorption spectroscopy (TDS) was carried out upon heating samples from room temperature to 800 °C at a heating rate of 20 °C s^{-1} in vacuum (10^{-5} Pa). In the TDS analysis, M/e (mass-to-charge ratio) = 18 peak that is attributed to H_2O was monitored to evaluate thermal stability of the porous film.

3. Results and discussion

In the initial study, the variations in refractive index and porosity of the porous silicate with processing temperatures are observed, as shown in Fig. 1. The porosity evolution during a series of baking and curing was determined through N_2 adsorption/desorption isotherm analysis. The as-spun film with a thickness of 380 nm had a refractive index of 1.19. After a baking at 150 °C, the water evaporated and the refractive index reduced to 1.17. In this thermal stage, thickness arised (~390 nm) because voids have been generated in the film. Then, the refractive index decreased further to 1.145 after the curing at 400 °C for 1 h. The thickness of the as-cured porous film also slightly increased to 400 nm. The significant decrease in the refractive index after a series of thermal processes was primarily caused by the elimination of the solvent and development of the porous structure. The refractive index of the porous film was obviously smaller than that of thermal oxide (~1.46). This result could predict that the dielectric constant of the porous silicate would be smaller than that of silicon dioxide.

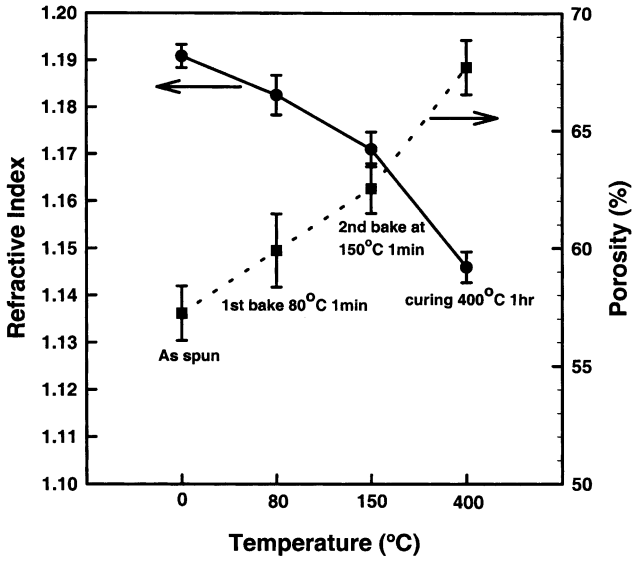

Fig. 1. Variations in refractive index and porosity of the porous silicate after a series of baking and curing steps.

Fig. 2 shows FTIR spectra of the porous silicate before and after a series of baking and curing steps. In the as-spun film, Si–OH bond exists approximately 3500 cm^{-1}, C–H peak at 2975 cm^{-1}, Si–C peak at 1273 cm^{-1}, Si–O bond at 1126 cm^{-1}. Since the porous film was synthesized from an organic precursor (TEOS) in methyl alcohol (CH_3OH) solvent and a surface modification with TMCS, carbon-containing chemical bonds such as R ($-CH_x$) and Si–R bonds appear in FTIR spectra. These chemical bonds are important functional groups characterizing the porous silicate film. After two baking processes, Si–OH peak intensity reduced due to the evaporation of the solvent. Sequentially, the peak of Si–OH bond disappeared and C–H bond decreased slightly after the curing at 400 °C.

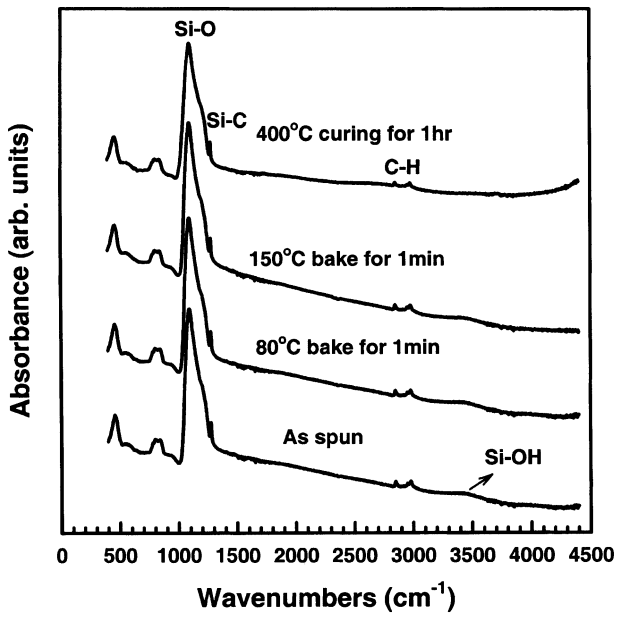

Fig. 2. FTIR spectra of the porous silicate before and after a series of baking and curing steps.

The electrical analysis was conducted to characterize the leakage current of the porous silicate. Various conduction mechanisms such as ohmic conduction, Schottky emission and Poole–Frenkel emission can be demonstrated using the MIS capacitor through $\ln J$–$E^{1/2}$ curve fitting [13,14], as shown in Fig. 3. In the low electrical field region, the leakage current density is nearly linear, as shown in Fig. 3a with a slope of 0.5 in the $\log J$ vs. $\log E$ plot. The linear portion of the $\log J$ vs. $\log E$ curve is typical of ohmic conduction in low electric field and is dependent on charged carriers such as electrons, holes and ions in the intrinsic porous film. A plot of the leakage current density versus the square root of the applied electric field gives a good representation of the leakage conduction behavior in the mid and high electric field, as shown in Fig. 3b and c. It is found that both leakage current densities are linearly related to the square root of the applied electric field. These linear variations of the current densities correspond either to Schottky emission or to the Poole–Frenkel mechanism [15].

The Schottky-emission generated by the thermionic effect is caused by electron transport across the potential energy barrier via field-assisted lowering at a metal–insulator interface. The current density (J) in the Schottky emission can be quantified by the following equation:

$$J = A^* T^2 \exp\left(\frac{\beta_s E^{1/2} - \phi_s}{k_B T}\right) \quad (1)$$

where $\beta_s = (e^3/4\pi\varepsilon_0\varepsilon)^{1/2}$, e the electronic charge, ε_0 the dielectric constant of free space, ε the high frequency relative dielectric constant, A^* effective Richardson constant, T absolute temperature, E the applied electric field, ϕ_s the contact potential barrier, and k_B the Boltzmann constant. Rearrangement of Eq. (1) results in a linear relationship between $\ln J$ and $E^{1/2}$:

$$\ln J = \frac{\beta_s}{k_B T}\sqrt{E} + \left[\ln(A^* T^2) - \frac{\phi_s}{k_B T}\right] \quad (2)$$

The Poole–Frenkel emission is due to field-enhanced thermal excitation of trapped electrons in the insulator into the conduction band. The current density is given

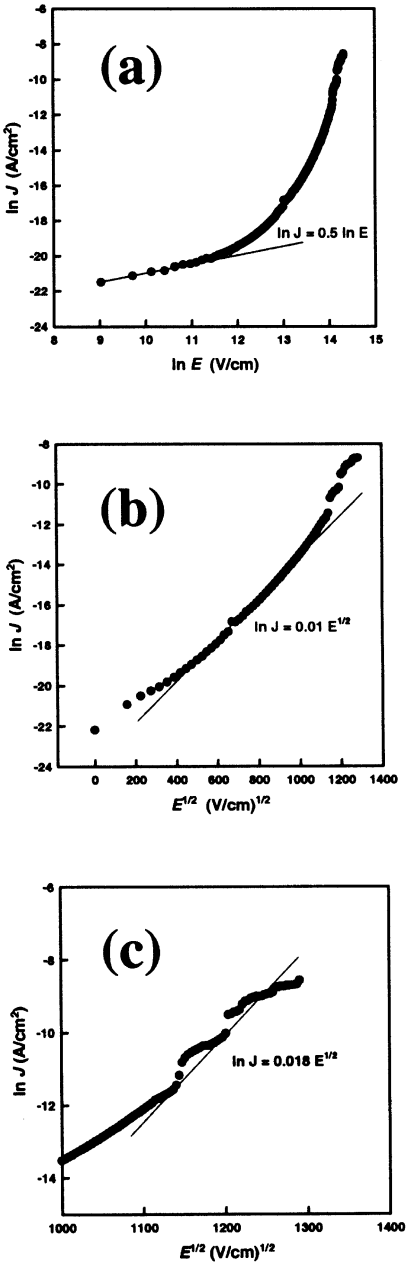

Fig. 3. Leakage current density (J) of porous silicate films as a function of electric field (E). (a) $\ln J$ vs. $\log E$ plot at the low electric field region and $\ln J$ vs. $E^{1/2}$ plot at the (b) mid and (c) high electric field region.

by

$$J = J_0 \exp\left(\frac{\beta_{PF} E^{1/2} - \phi_{PF}}{k_B T}\right) \quad (3)$$

where $J_0 = \sigma_0 E$ is the low-field current density, σ_0 the low-field conductivity, $\beta_{PF} = (e^3/\pi\varepsilon_0\varepsilon)^{1/2}$, ϕ_{PF} the height of trap potential well. For trap states with coulomb potentials, the expression is virtually identical to that of the Schottky emission. The barrier height, however, is the depth of the trap potential well, and the quantity is larger than in the case of Schottky emission by a factor of 2 [15]. Rearrangement of Eq. (3) also yield a linear relationship between $\ln J$ and $E^{1/2}$ given by

$$\ln J = \frac{\beta_{PF}}{k_B T}\sqrt{E} + \left[\ln(J_0) - \frac{\phi_{PF}}{k_B T}\right] \quad (4)$$

The two processes can be distinguished by comparing the theoretical value of β with the calculated one obtained from the slope of the experimental curve $\ln J$–$E^{1/2}$. The relative dielectric constant determined from capacitance measurements of samples with the Al-gate is approximately 1.7 at room temperature. The slope $(\beta/k_B T)$ of the straight-line portion of curve in Fig. 3b and c gives a value of 4.56×10^{-23} in the mid electric field region, 7.725×10^{-23} $J(m/V)^{1/2}$ in high electric field region for β, respectively. The theoretical value of β_S and β_{PF} are 4.64×10^{-23} and 9.28×10^{-23} $J(m/V)^{1/2}$, respectively. From these results, the transport mechanisms of carriers in the porous silicate film could be summarized by the Schottky emission in the mid electric field region. As the applied electric field increases, the transport mechanism gradually transforms into Poole–Frenkel emission. The reason might be that the increasing electric field will brake the bonding and lead to an increase of the dangling bonds (or trapping sites) in the porous silicate. The resultant traps tend to enhance Poole–Frenkel type conduction mechanism.

Thermal stability is a critical consideration for the use of the porous material. In this work the thermal stability of the porous film was investigated by varying thermal annealing temperatures. Fig. 4a shows that the variation of the porous silicate thickness for annealing temperatures ranging from 350 to 600 °C. A significant decrease in film thickness is observed after the thermal annealing at 600 °C. In addition, Fig. 4b shows that the refractive index increased from 1.144 to 1.156 as the annealing temperature increase from 350 to 600 °C, while the porosity decreased from 68.8 to 65.7%. It seems that a modification to the porous film structure might have occurred leading to dielectric degradation. FTIR spectra of porous films with various annealing temperatures were obtained in order to interpret this phenomenon. As shown in Fig. 5, the intensities of the

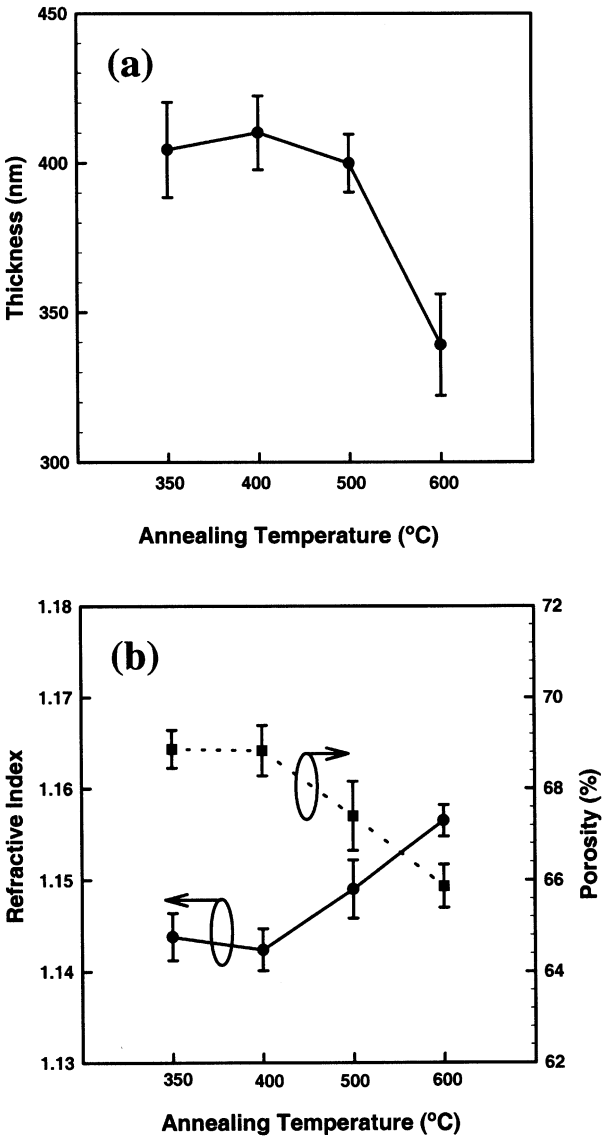

Fig. 4. (a) Thickness variation of the porous silicate films with different annealing temperatures. (b) The variations in refractive index and porosity of porous silicate films with different annealing temperatures.

functional groups in FTIR spectra did not change significantly after thermal annealing at 350, 400, and 500 °C. However, a significant change occurred after annealing at 600 °C. The intensities of Si–C and C–H bonds decreased and H–OH peak abruptly increased. Decomposition of some functional groups resulted in a dramatic shrinking of the film thickness and a reduction of the porosity.

Dielectric properties of the porous films were further investigated to verify the impact of the decomposition of some functional groups on electrical characteristics of the films. Fig. 6a and b show the dielectric constant and leakage current of the porous films after different

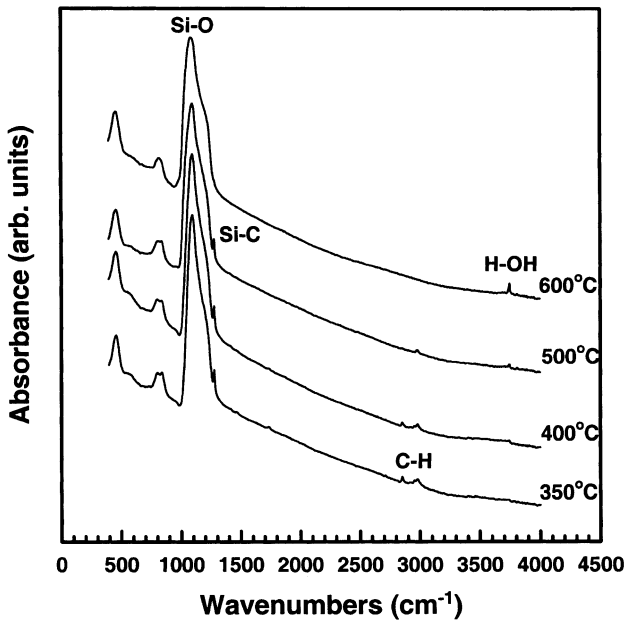

Fig. 5. FTIR spectra of porous films with various annealing temperatures for 1 h.

thermal annealing. Dielectric constant of the porous silicate with k value of 1.7 was maintained up to 500 °C. Once annealing temperature is increased to 600 °C, dielectric degradation occurred. The dielectric constant increased up to 3.7. The same evolution with temperatures appeared in the leakage current behavior of thermally annealed porous films. The leakage current of the porous films was constant below 500 °C. However, leakage current significantly increased after thermal annealing at 600 °C. These electrical degradations are attributed to the destruction of functional groups and the formation of Si–OH bonds after the elevated annealing temperature. The polarity Si–OH bonds would make the porous film to easily absorb moisture and result in the increase in both dielectric constant and leakage current.

The moisture desorption of the porous films with different annealing temperatures were compared from the TDS analysis. In Fig. 7, the evolution of the moisture content is compared for the samples annealed at 350, 400, 500, and 600 °C. The kinetics of moisture desorption from spin-on-glass film has been studied previously [16]; the first desorption peak at ~200 °C was attributed to moisture adsorbed at the film surface, and the second peak at 400–600 °C was attributed to moisture tightly bonded through Si–OH groups at the internal surface of porous silicate films [17]. In this work, the most significant moisture outgassing is observed for the 600 °C-annealed sample. This confirms previous inference on electrical deterioration. The electrical and material characterization seem to indicate that the low-k quality of the porous film is maintained up to 500 °C.

4. Conclusions

A novel siloxane-based porous film was successfully fabricated and presented a very low dielectric constant (~1.7). The conduction mechanisms for leakage current were determined as being ohmic conduction in low electric field, Schottky emission in mid electric field,

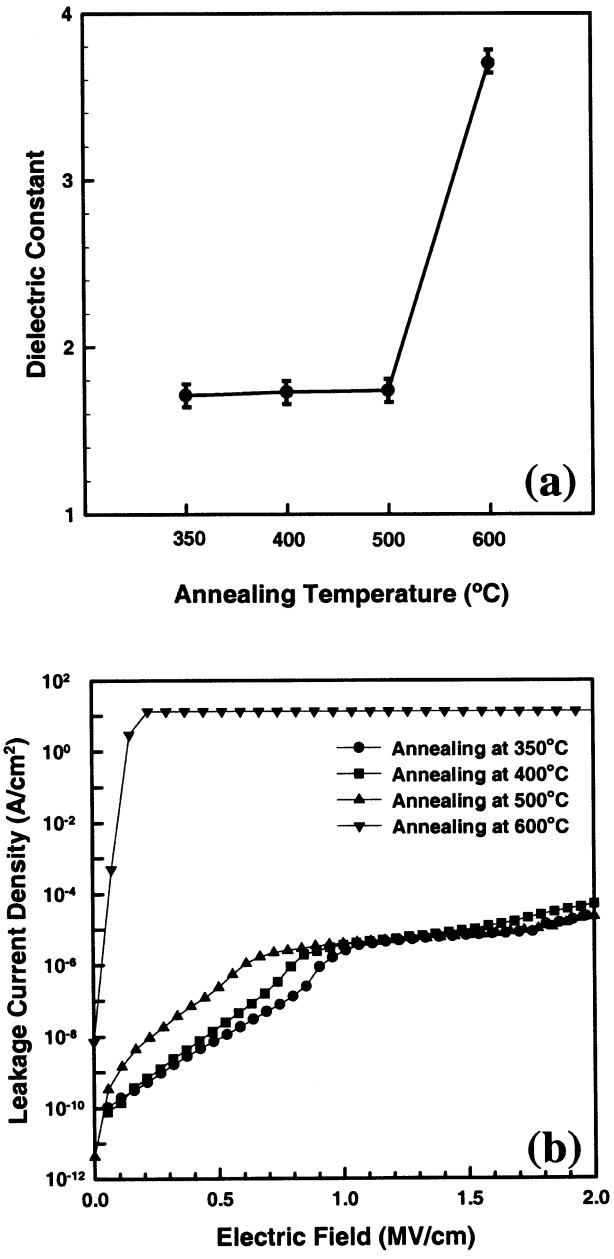

Fig. 6. Dielectric properties of porous silicate films after various thermal annealing treatments at 350, 400, 500 and 600 °C for 1 h. (a) Dielectric constant of porous silicate films. (b) Leakage current density of porous silicate film as a function of electric field.

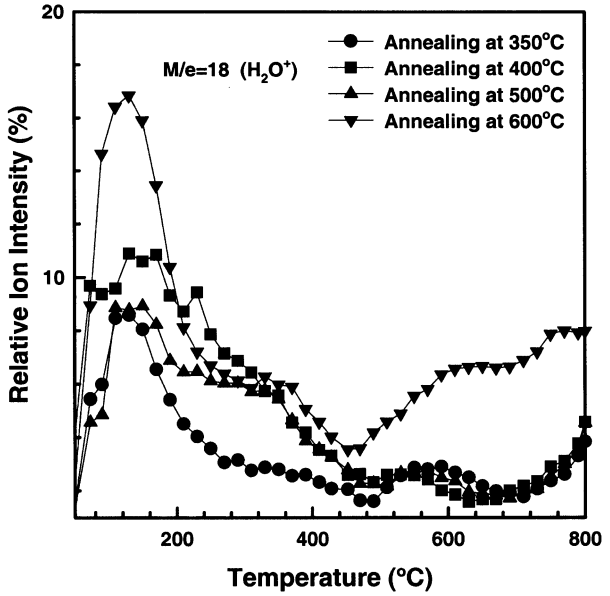

Fig. 7. Temperature dependence of moisture ($M/e=18$) desorption from porous silicate films with various annealing treatments for 60 min.

and Poole–Frenkel emission in high electric field. Since the porous film was synthesized from an organic precursor in methyl alcohol solvent, the carbon-containing chemical bonds dominate the dielectric properties of the porous film. A lower film density (~ 0.6 g cm^{-3}) and substitution of Si–C for high polarized Si–O are the main reason for the decrease in the dielectric constant. In this study, the qualities of the porous silicate film such as shrinkage and thermal stability have been found to be dependent on the presence of organic functional groups. Below 500 °C annealing temperature, a certain amount of Si–C bonds are still present. The presence of these functional groups explain low-k characteristics of the porous silicate film.

Acknowledgments

This work was performed at the National Nano Device Laboratory and was supported by the National Science Council of the Republic of China under Contract, No. NSC 90-2721-2317-200.

References

[1] R.H. Dennard, F.H. Gaensslen, H.N. Yu, V.L. Rideout, E. Bassous, A.R. LeBlanc, IEEE J. Solid-State Circuits SC-9 (1974) 256.
[2] M.T. Bohr, IEDM Tech. Dig. Washington DC (1995) 241.
[3] The National Technology Roadmap for Semiconductors, Semiconductor Industry Association, San Jose, CA, 1997.
[4] G. Sugahara, N. Aoi, M. Kubo, K. Arai, K. Sawada, International Dielectrics for ULSI Multilevel Interconnection Conference, (1997) 19.
[5] P.T. Liu, T.C. Chang, S.M. Sze, F.M. Pan, Y.J. Mei, W.F. Wu, M.S. Tsai, B.T. Dai, C.Y. Chang, F.Y. Shih, H.D. Hung, Thin Solid Films 332 (1998) 345.
[6] P.T. Liu, T.C. Chang, Y.S. Mor, S.M. Sze, Jpn J. Appl. Phys. 38 (1999) 3482.
[7] R.D. Miller, R. Beyers, K.R. Carter, R.F. Cook, M. Harbison, C.J. Hawker, J.L. Hedrick, V. Lee, E. Liniger, C. Nguyen, J. Remenar, M. Sherwood, M. Trollsas, W. Volksen, D.Y. Yoon, Mater. Res. Soc. Symp. Proc. 565 (1999) 3.
[8] P.T. Liu, C. Chang, Y.S. Mor, C.W. Chen, T.M. Tsai, C.J. Chu, F.M. Pan, S.M. Sze, Electrochem. Solid-State Lett. 5 (2002) G11.
[9] C. Jin, J.D. Luttmer, D.M. Smith, T. Ramos, MRS Bull. 22 (1997) 39.
[10] Y.P. Tsai, C.N. Liao, Y. Xu, K.N. Tu, B. Zhao, Q.Z. Liu, M. Brongo, Mater. Res. Soc. Symp. Proc. 565 (1999) 17.
[11] P. Singer, Semiconductor Int. 19 (1996) 88.
[12] J.K. Hong, H.S. Yang, M.H. Jo, H.H. Park, S.Y. Choi, Thin Solid Films 308–309 (1997) 495.
[13] P.T. Liu, T.C. Chang, Y.L. Yang, Y.F. Cheng, S.M. Sze, IEEE Trans. Electron Devices 47 (2000) 1733.
[14] H.S. Yang, S.Y. Choi, S.H. Hyun, C.G. Park, Thin Solid Films 348 (1999) 69.
[15] S.M. Sze, Physics of Semiconductor Devices, Wiley, New York, 1981, Chapter 7.
[16] J. Proost, E. Kondoh, G. Vereecke, M. Heyns, K. Maex, J. Vac. Sci. Technol. B 16 (1998) 2091.
[17] E. Kondoh, M.R. Baklanov, H. Bender, K. Maex, Electrochem. Solid-State Lett. 1 (1998) 224.